Biosensors and Bioelectronics 127 (2019) 174–180

Contents lists available at ScienceDirect

Biosensors and Bioelectronics

journal homepage: www.elsevier.com/locate/bios

Label-free immunosensors based on a novel multi-amplification signal strategy of TiO_2-NGO/Au@Pd hetero-nanostructures

Qin Yan[a,1], Linlin Cao[b,1], Hui Dong[a], Zhaoling Tan[a], Yitian Hu[a], Qing Liu[a,*], Hui Liu[a], Pingping Zhao[c], Lei Chen[a], Yuying Liu[a], Yueyun Li[a], Yunhui Dong[a]

[a] School of Chemistry and Chemical Engineering, Shandong University of Technology, Zibo 255049, PR China
[b] Department of Clinical Laboratory, Zibo Central Hospital, Zibo 255036, PR China
[c] College of Chemical and Environmental Engineering, Shandong University of Science and Technology, PR China

ARTICLE INFO

Keywords:
Label-free electrochemical immunosensor
Titanium oxide
Nitrogen-doped reduced graphene oxide
Au@Pd nanoparticles
Human epididymis specific protein 4

ABSTRACT

A label-free electrochemical immunosensor for quantitative detection of human epididymis specific protein 4 antigen (HE4 Ag) was developed by a novel multi-amplification signal system. The multi-amplification signal system was formed by loading bimetallic Au@Pd holothurian-shaped nanoparticles (Au@Pd HSs) on titanium oxide nanoclusters functionalized nitrogen-doped reduced graphene oxide (TiO_2-NGO). The Au@Pd HSs were obtained via seed-mediated approach with in-situ grown palladium nanoarms on gold nanorods (Au NRs) surfaces, which possessed good electrocatalysis for hydrogen peroxide (H_2O_2) reduction and excellent biocompatibility. The TiO_2-NGO with the high catalytic activity and large specific surface area was synthesized by hydrothermal method. Using H_2O_2 as an electrochemically active substrate, the prepared label-free electrochemical immunosensor based on the TiO_2-NGO/Au@Pd HSs hetero-nanostructures as the signal amplification platform exhibited excellent selectivity, reproducibility and stability for the detection of HE4 Ag. Meanwhile, the linear range from 40 fM to 60 nM with the detection limit of 13.33 fM (S/N = 3) was obtained, indicating the immunosensor offers a promising method for clinical detection of HE4 Ag.

1. Introduction

Epithelial ovarian cancer with the highest mortality rate in gynecological diseases is one of the most common malignant tumors, threatening human health and quality of life (Mathieu et al., 2017; Zhang et al., 2003). Given ovarian cancer as an asymptomatic disease clinically (Lu, 2018), it is easy to cause the missed diagnosis and misdiagnosis, which is a tricky problem in early diagnosis. Human epididymis specific protein 4 antigen (HE4 Ag) as one of the most promising new tumor markers of ovarian cancer has high sensitivity and specificity, which can help to early diagnose and monitor disease recurrence (Anastasi et al., 2010; Capriglione et al., 2017). Therefore, the development of a sensitive, simple and rapid analytical method for timely screening and monitoring of HE4 Ag is an effective way to decrease the mortality.

Electrochemical immunosensor based on the biospecific recognition between the antigens and corresponding antibodies has been widely applied in analytical biochemistry owing to their combined merits of being easy to operate, cost-effective and pollute-free (Felix and Angnes, 2017; L. Li et al., 2018). Especially, label-free electrochemical immunosensor has attracted considerable interest among researchers because of its good sensitivity and rapid detection (Okuno et al., 2007; R. Wang et al., 2017; Wei et al., 2012). However, the electrochemically active substrate (i.e., hydrogen peroxide (H_2O_2)) is needed for immunosensors, since immune proteins (antigen or antibody) are not intrinsically able to act as redox partners in immunoassay reaction. For label-free electrochemical immunosensor, the electrical signal is performed by using different nanomaterials as signal amplification platform conjugated with immune proteins to catalyze H_2O_2 (Berggren and Johansson, 1997; R. Wang et al., 2017; Yan et al., 2018). Therefore, it is significant to construct a highly sensitive immunosensor by preparing an effective material with good catalytic properties for the reduction of H_2O_2.

Recently, various promising nanomaterials with the outstanding catalytic properties or electrical conductivity are used as the signal amplification platform to decrease the detection limit and increase sensitivity of the immunosensor (Samanman et al., 2015), such as noble metal nanomaterials, metal oxides, carbon materials and so on (Li et al.,

* Corresponding author.
E-mail address: qingliu0315@163.com (Q. Liu).
[1] These authors contributed equally to this work.

https://doi.org/10.1016/j.bios.2018.12.038
Received 15 October 2018; Received in revised form 7 December 2018; Accepted 10 December 2018
Available online 27 December 2018
0956-5663/

2017; Rauf et al., 2018a, b; Sengottaiyan et al., 2017; Y. Yang et al., 2017). Among these nanomaterials, hetero-nanostructures with excellent conductivity and high catalytic ability have attracted considerable interest because of their synergistic effect (Kim et al., 2016; Yang et al., 2013). Gold nanoparticles (Au NPs) are considered as striking noble metal such as gold nanorods (Au NRs) and gold nanospheres (Au NSs), which have good biocompatibility, conductivity and stability (Daniel and Astruc, 2004; Kim et al., 2017). Palladium nanoparticles (Pd NPs) are known to have good electrocatalytic activities toward H_2O_2 (Chen et al., 2013). In particular, Au NRs are conducive to the growth of palladium nanoclusters with high crystal surface index, which can further improve the electrocatalysis towards the reduction of H_2O_2 (Tran and Lu, 2011; Wang et al., 2011). Therefore, bimetallic Au@Pd holothurian-shaped nanocomposites (Au@Pd HSs) could have superior catalytic activity and good biocompatibility because of their synergistic effect.

As is known to us all, metal materials are generally dispersed on supporting material to obtain nanocomposites with good biocompatibility, high conductivity and excellent catalytic properties (Yang et al., 2016). Nitrogen-doped reduced graphene oxide (NGO) has attracted much attention as robust catalyst supports owing to the advantages of excellent electroconductivity, high specific surface area and good chemical tolerance (Emran et al., 2017b, 2018a, b; Kaur et al., 2018; Dal Magro et al., 2018). In recent years, doped metal-oxide semiconductors into carbon materials, such as nickel oxide, copper oxide, ceric oxide and titanium oxide Akhtar et al., 2015, 2016; Akhtar and Shenashen, 2017; Emran et al., 2017a; Wei et al., 2016b), are promising in the immunosensor functionality attributed to their good biocompatibility and unique physical and chemical properties. We reduced Ti^{4+} in suit into NGO via one-pot hydrothermal method to form the ultrafine titanium oxide (TiO_2) doped NGO (TiO_2-NGO), which not only has elevated water solubility ascribed to the introduction of hydrophilic TiO_2 nanocrystals, but also has good catalytic properties thanks to the high-index face of TiO_2 clusters (Chen and Mao, 2007; Nosrati et al., 2017; Yao et al., 2018). The well-dispersed TiO_2-NGO can act as buffer space to support noble metal nanoparticles owing to its high active surface area and good chemical stability (Ghasemi et al., 2013). Meanwhile, 3-aminopropyl triethoxysilane (APTES) modified TiO_2-NGO can enhance the loading capacity of noble metal and stability of the immunosensor, due to stable conjunction between noble metal nanoparticles and amino groups (Wei et al., 2016a). Therefore, Au@Pd HSs acting as a bridge to incubate with antibody by Au—N or Pd—N bond (H. Wang et al., 2017; Zhou et al., 2014) were decorated on APTES modified TiO_2-NGO nanocomposites (TiO_2-RGO/Au@Pd HSs) as a signal amplification platform simultaneously enhancing the sensitivity of immunosensor.

In this work, a novel TiO_2-NGO/Au@Pd HSs hetero-nanostructure was used to construct a label-free electrochemical immunosensor for the quantitative detection of human epididymis specific protein 4 antigen (HE4 Ag). On one hand, Au@Pd HSs have good biocompatibility and excellent electrocatalytic activity, which can immobilize antibodies effectively and promote the reduction of H_2O_2. On the other hand, TiO_2-NGO exhibits a significantly enhanced electrocatalytic performance towards H_2O_2 reduction and has a large specific surface area to further realize signal amplification. Due to the synergistic effect between the TiO_2-NGO and Au@Pd HSs, the designed label-free electrochemical immunosensor has a wide detection range, high sensitivity and low detection limit for HE4 Ag detection, which provides a promising platform for clinical screening of cancer biomarkers and point-of-care assays.

2. Experimental section

2.1. Fabrication of the immunosensor

In order to explain the preparation process of working electrode clearly, Fig. 1 shows the stepwise self-assembly procedure. The preparation procedure of the Au@Pd HSs (a), and TiO_2-NGO/Au@Pd HSs (b) was exhibited in Supplementary material (SM). The glassy carbon electrode (GCE, 4 mm in diameter) was carefully polished with 50 nm alumina powders, and washed thoroughly with ultrapure water to obtain a fresh and mirror-like surface. Then, the TiO_2-NGO/Au@Pd HSs modified electrode (TiO_2-NGO/Au@Pd HSs/GCE) was obtained by dropping TiO_2-NGO/Au@Pd HSs (6 μL, 2.5 mg mL^{-1}) composite onto the surface of the pretreated working electrode. After the TiO_2-NGO/Au@Pd HSs/GCE dried, HE4 antibody solution (anti-HE4, 6 μL, 10 μg mL^{-1}) was incubated on the surface of TiO_2-NGO/Au@Pd HSs/GCE and dried at 4 °C. After washing, bovine serum albumin solution (BSA, 3 μL, 1 wt%) was coated onto the anti-HE4/TiO_2-NGO/Au@Pd HSs/GCE to eliminate possible remaining active sites between the substrate material and HE4 antigen (HE4 Ag). After 1 h incubation, the BSA/anti-HE4/TiO_2-NGO/Au@Pd HSs/GCE was rinsed with phosphate buffered solutions (PBS, pH = 7.0) and incubated with different concentrations of HE4 Ag (6 μL, 40 fM to 60 nM) for 40 min to ensure the specific binding between HE4 Ag and anti-HE4. Finally, the modified working electrode was rinsed with PBS and stored in 4 °C for further measurement.

2.2. Electrochemical measurements

Electrochemical measurements were performed on CHI760E electrochemical workstation (Shanghai CH Instruments Co., China) at a standard three-electrode system including a platinum wire electrode as auxiliary, a saturated calomel reference electrode (SCE) as reference electrode and a modified electrode as working electrode. Amperometric i-t curve measurement of the immunosensor was carried out at −0.4 V as the scan potential. When the background current retained stable under smooth stirring, H_2O_2 (10 μL, 5 M) was injected into the PBS (10 mL, pH = 7.4) and then the current response change was recorded. Cyclic voltammetry (CV) experiments were performed in potassium ferricyanide ($K_3[Fe(CN)_6]$, 5 mM). Electrochemical impedance spectroscopy (EIS) were monitored in a solution containing potassium chlorate (KCl, 0.1 M) and 2.5 mM $Fe(CN)_6^{3-}/Fe(CN)_6^{4-}$ for representing the interfacial properties of modified electrode. All electrochemical measurements were performed at room temperature.

3. Results and discussion

3.1. Characterization of Au NRs, Au@Pd HSs, NGO, TiO_2-NGO and TiO_2-NGO/Au@Pd HSs nanocomppsites

Fig. 2A shows the TEM image of the Au NRs. Clearly, the obtained Au NRs have an average length of 36 nm and width of 12 nm with an aspect ratio of 3 and their size distribution is relatively uniform. It can be found that the Au@Pd HSs appear in macelike nanostructures, where inner Au NR cores are homogeneously surrounded by Pd nanoarms shells. Furthermore, the scanning transmission electron microscope (STEM) mapping images of Au@Pd HSs (Fig. S1A–D) with the distribution of Au and Pd elements prove the formation of the core-shell nanostructures. EDX spectrum of Au@Pd HSs (Fig. S1E) indicates that the elements contained in the prepared nanocomposites are Au and Pd.

The TEM and Raman spectroscopy of NGO and TiO_2-NGO are compared in Fig. 2C–E. Evidently, the NGO has a typical graphene thin wrinkled paper-like structure (Fig. 2C). After doping TiO_2, there are many dark dots with the average diameter of 8.5 nm distributed uniformly on the surface of layered paper-like structure. This indicates that ultrafine TiO_2 clusters have been successfully reduced on NGO (Fig. 2D). HRTEM microscopy image (inset in Fig. 2D) of TiO_2 shows a high degree of crystallinity with the interplanar distance of 0.35 nm, possibly ascribed to the plane of crystal TiO_2 (101) (Qamar et al., 2017; Zhang et al., 2018). Raman spectroscopy has played an important role in the characterization of graphitic materials. As shown in Fig. 2E, NGO (black curve) has the characteristic peaks of carbon materials, namely D

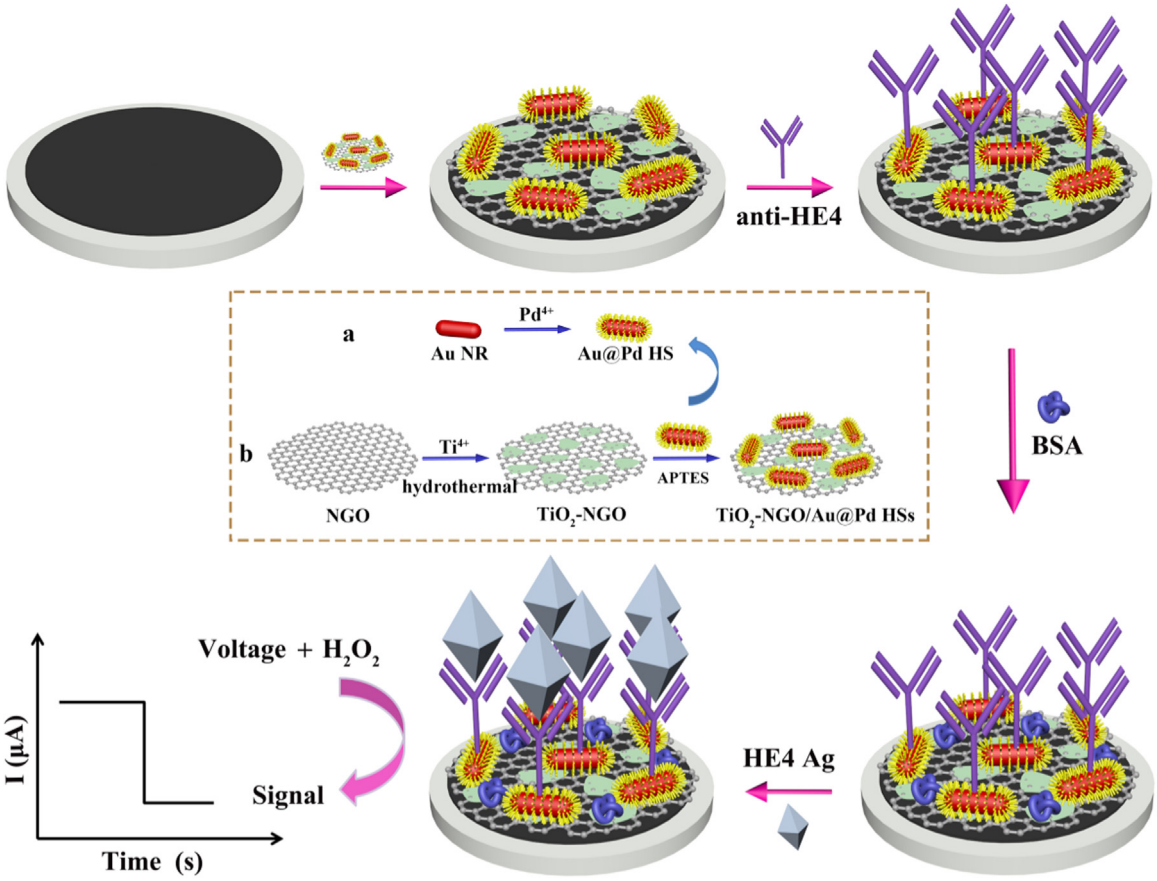

Fig. 1. Fabrication for working electrode of the label-free immunosensor. The preparation procedure of the Au@Pd HSs (a), and the building-up process of the TiO_2-NGO/Au@Pd HSs (b).

band (1354 cm^{-1}) and G band (1613 cm^{-1}) respectively (Liu et al., 2018). I_D/I_G ratio of NGO is 1.1, indicating a higher distortion in the carbon materials due to the doped nitrogen (Z. Yang et al., 2017). In contrast, after hydrothermal reaction between NGO and titanium (IV) isopropoxide (TTIP, red curves), the Raman spectrum shows the characteristic peaks of TiO_2 at 0–800 cm^{-1} (inset in Fig. 2E, red curve), representing E_{g1} band (145 cm^{-1}), E_{g1} band (400 cm^{-1}), B_{1g} band (516 cm^{-1}) and A_{1g} band (641 cm^{-1}), respectively (Balachandran and Eror, 1982; Swamy et al., 2005). This result also proves that the structure of NGO doped with TiO_2 is successfully prepared. In addition, C, O, N, and Ti elements are observed in the EDX of TiO_2-NGO (Fig. 2F), which further demonstrates that the TiO_2-NGO composites are successfully synthesized. Moreover, FT-IR spectrums of NGO, TiO_2-NGO and APTES modified TiO_2-NGO are compared in Fig. S1F, which demonstrate the TiO_2 nanoclusters and APTES were successfully modified onto NGO in turn. The N_2 adsorption-desorption isotherm of the TiO_2-NGO proved that the large surface area was 160.86 m^2 g^{-1} and the total pore volume was 0.47 cm^3 g^{-1}, which facilitated TiO_2-NGO as a superior support for the Au@Pd HSs (Fig. S2A).

The TEM images and EDX of the TiO_2-NGO/Au@Pd HSs are shown in Fig. 2G–I. It is obvious that the Au@Pd HSs are attached on the TiO_2-NGO (Fig. 2G and H). Both the EDX analysis (Fig. 2I) and the STEM mapping images (Fig. S3A–I) detected C, O, N, Ti, Si, Au and Pd elements, which clearly confirmed that the TiO_2-NGO/Au@Pd HSs are prepared successfully. The thermogravimetric analysis (TGA) of the samples TiO_2-NGO/Au@Pd HSs was performed in Fig. S2B, indicating that the prepared material has good thermal stability.

3.2. The mechanism of multiple signal amplification

The proposed label-free electrochemical immunosensor has good catalytic activity and conductivity, relying on the synergistic effect of various fabricating materials. To investigate the signal amplification mechanism of the TiO_2-NGO/Au@Pd HSs, control experiments of different nanomaterials modified GCE was performed. As is shown in Fig. 3A, NGO, TiO_2 NPs, Au NRs, TiO_2-NGO, APTES modified TiO_2-NGO, Au@Pd HSs and TiO_2-NGO/Au@Pd HSs (2.5 mg mL^{-1}, 6 μL) were carried out for the reduction of 5 mM H_2O_2 under − 0.4 V in PBS at pH = 7.4. It can be observed that NGO (curve a), TiO_2 NPs (curve b), have slight electrocatalytic current response, indicating that the NGO and TiO_2 have no obvious electrocatalytic properties towards the reduction of H_2O_2. The TiO_2-NGO has improved catalytic performance towards the reduction of H_2O_2 (curve d), which is attributed to the fine TiO_2 nanoclusters with high surface area and activity (Yu et al., 2016). Compared with Au NRs (curve b), the Au@Pd HSs (curve f) have enhanced catalytic properties. Moreover, the current response of the APTES modified TiO_2-NGO (curve e) and the TiO_2-NGO is similar. To further improve the signal of the immunosensor, the TiO_2-NGO/Au@Pd HSs (curve g) were synthesized by loading the Au@Pd HSs with good electrocatalytic activity and conductivity on TiO_2-NGO, which displayed the highest current response. This expected result is attributable to the following points. Firstly, the bimetallic Au@Pd HSs have good electrical conductivity and can promote the electron transfer rate between the working electrode and the electrolyte solution. Secondly, the synergetic catalysis and intimate electronic interactions between Au@Pd HSs and TiO_2-NGO make the TiO_2-NGO/Au@Pd HSs nanocomposites possess well-developed capability for H_2O_2 reduction.

A.C. impedance method is an effective way to detect the features of

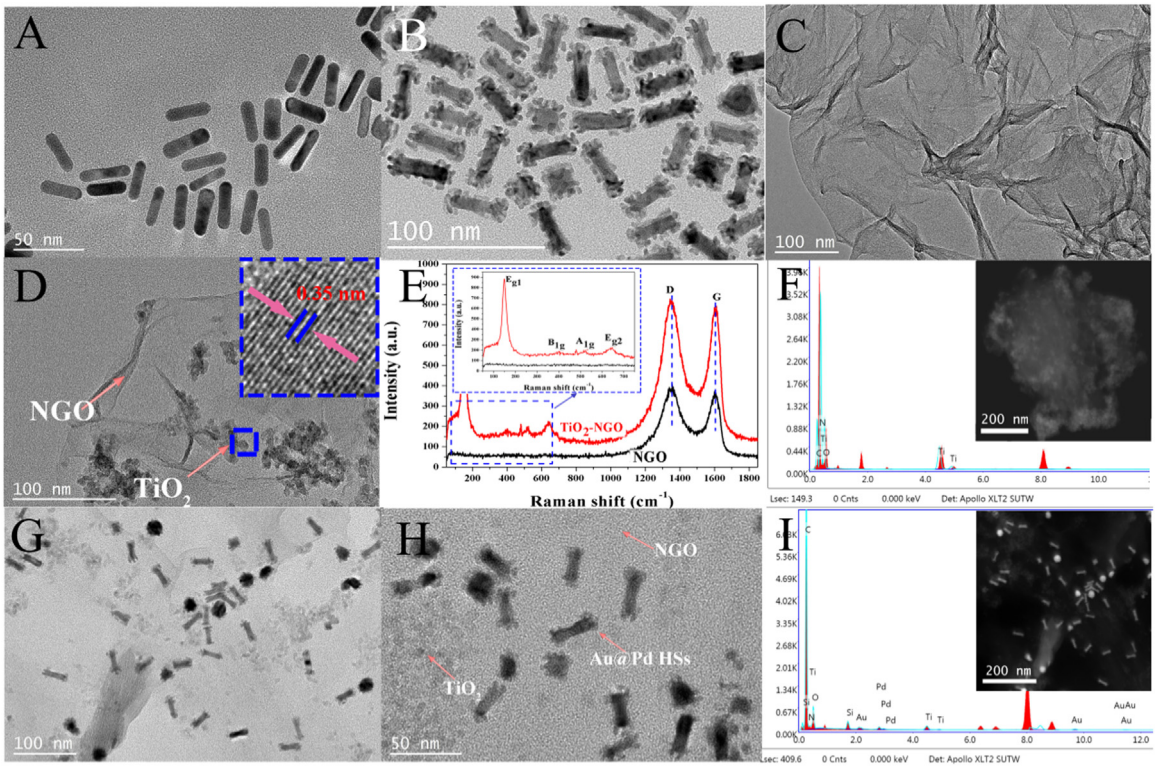

Fig. 2. TEM images of Au NRs (A), Au@Pd HSs (B), NGO (C) and TiO_2-NGO (D); Raman spectroscopy of NGO and TiO_2-NGO (E); EDX spectrum of TiO_2-NGO (F); TEM image of TiO_2-NGO/Au@Pd HSs (G) and (H); EDX spectrum of TiO_2-NGO/Au@Pd HSs (I). (For interpretation of the references to color in this figure, the reader is referred to the web version of this article.)

surface-modified electrodes (Alarfaj et al., 2018; F. Li et al., 2018). Nyquist plots of A.C. impedance spectroscopy consist of two parts: a semicircle diameter with high frequencies corresponding to the electron-transfer resistance (R_{et}) correlated with modification of the electrode surface, and a linear portion with low frequencies indicating the electron transfer limited process. In brief, R_{et} can be judged by observing the diameter change of semicircle portion. Inset in Fig. 3B illustrates the Randles equivalent circuit, which includes the R_{et}, resistance of solution (R_s), constant phase angle element (CPE) and the Warburg impedance (Z_w). A good fit relationship was obtained using ZView-Impedance Software and the relevant data are shown in Table S1. As is shown in Fig. 3B, NGO (curve b) and Au@Pd HSs (curve e) have better conductivity than bare GCE (curve a). The R_{et} of TiO_2-NGO/GCE (curve c) is slightly larger than that of bare GCE, which may be due to the fact that TiO_2 is a semiconductor. When TiO_2-NGO modified by the APTES was dripped onto GCE surface (curve d), the value of R_{et} was larger than of TiO_2-NGO/GCE, indicating the APTES was successfully modified on TiO_2-NGO. When Au@Pd HSs are further modified onto the TiO_2-NGO-APTES/GCE surface (curve f), the R_{et} decreased sharply because the Au@Pd HSs have good conductivity.

To demonstrate the prepared TiO_2-NGO/Au@Pd HSs hetero-nanostructures have good electrical conductivity, heterogeneous electron transfer rate constant (k_s) is used to characterize the electron transport properties. Fig. 3B shows the CV measurement of TiO_2-NGO/Au@Pd HSs/GCE in 5 mM $K_3[Fe(CN)_6]$ at different scan rates. It can be seen that with the increase of scan rates, the oxidation peak shifts to more positive potentials, while the reduction peak shifts to more negative potentials. A linear relationship between peak potentials and denary logarithm of scan rate (lg υ) is observed at the scan rates ranging from 500 mV s^{-1} to 900 mV s^{-1}, which is in agreement with the Laviron theory (Laviron and Roullier, 1980): a plot of E_p versus lg υ (Fig. 3C) yields two straight lines with slopes of $2.3RT/(1-\alpha)nF$ (ka) for the anodic peak and $-2.3RT/\alpha nF$ (kc) for the cathodic peak. Therefore, the charge-transfer coefficient (α) can be estimated as 0.55 from the slope of the straight lines based on the equation (Eq. (1)). The k_s was estimated to be 1.11 s^{-1} using the Laviron model equation (Eq. (2)) (Laviron, 1979) as follows:

$$\log\frac{ka}{kc} = \log\left(\frac{\alpha}{1-\alpha}\right) \tag{1}$$

$$\log k_s = \alpha\log(1-\alpha) + (1-\alpha)\log\alpha - \log\frac{RT}{nF\upsilon} - \frac{\alpha(1-\alpha)nF\Delta E_p}{2.3RT} \tag{2}$$

where ΔE_p is peak separation, υ is scan rate (mV s^{-1}), F is Faraday constant (96,485 C mol^{-1}), n is the number of transferred electrons (n = 1), R is gas constant (8.314 J K^{-1} mol^{-1}) and T is the absolute temperature (298 K). The value of k_s is higher than that of other nanoparticles based electrochemical biosensor (Li et al., 2015; Zhang et al., 2006; Zhao et al., 2005), indicating fast electron transfer between TiO_2-NGO/Au@Pd HSs hetero-nanostructures and electrode. Therefore, the TiO_2-NGO/Au@Pd HSs hetero-nanostructures were used as signal amplification platform to fabricate an amperometric label-free immunosensor with high sensitivity.

3.3. Characterization of the immunosensor

A.C. impedance method was performed for probing the electrical properties of biological interfaces, and the fitting parameters of the modified electrode are shown in Table S2. As is shown in Fig. 4A, when TiO_2-NGO/Au@Pd HSs hetero-nanostructures were modified onto the bare GCE, the Ret (curve b) greatly decreased than that of the bare GCE (curve a), indicating that TiO_2-NGO/Au@Pd HSs hetero-nanostructures can provide good conductivity. Furthermore, the Ret successively increased after its self-assembly with the anti-HE4 (curve c), BSA (curve d) and HE4 Ag (curve e), which indicated the successful modification of

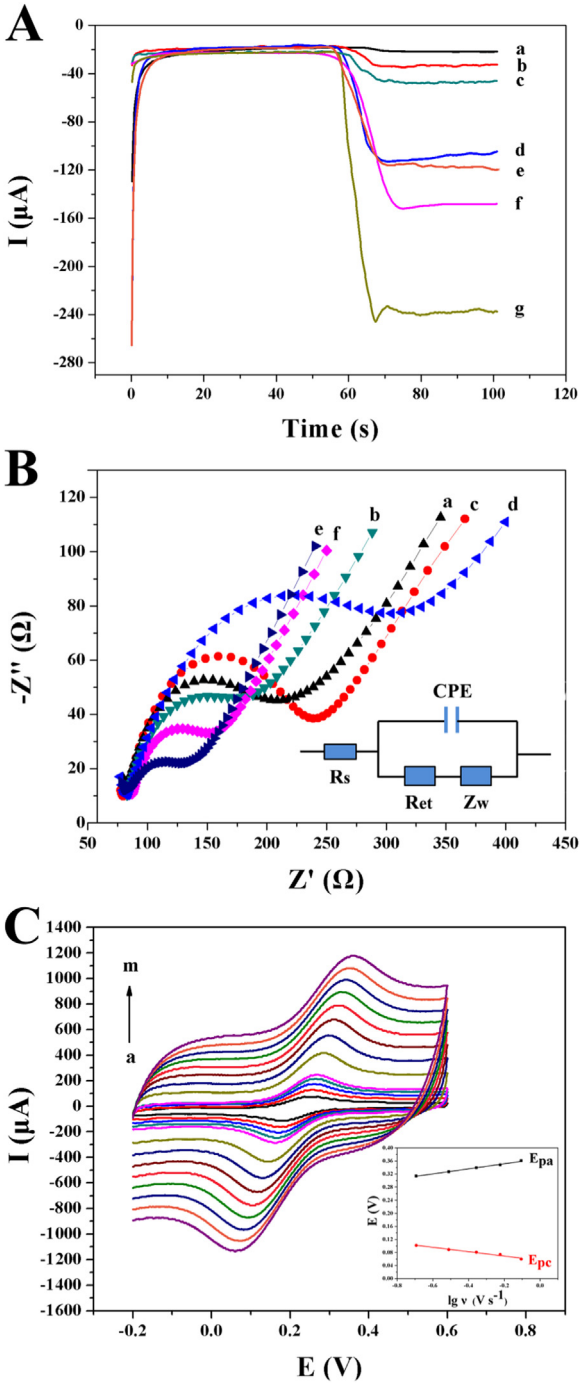

Fig. 3. (A) Amperometric responses of different modified electrodes in PBS (pH = 7.4): (a) NGO, (b) TiO_2 NPs, (c) Au NRs, (d) TiO_2-NGO, (e) APTES modified TiO_2-NGO, (f) Au@Pd HSs and (g) TiO_2-NGO/Au@Pd HSs; (B) A.C. impedance measurement of different materials in a solution containing 0.1 M KCl and 2.5 mM $Fe(CN)_6^{3-/4-}$ at potential of 0.27 V with frequency range of 1–10^5 Hz: (a) bare GCE, (b) NGO, (c) TiO_2-NGO, (d) APTES modified TiO_2-NGO, (e) Au@Pd HSs, (f) TiO_2-NGO/Au@Pd HSs; (C) Influence of scan rate on electrochemical responses of TiO_2-NGO/Au@Pd HSs/GCE in 5 mM $K_3[Fe(CN)_6]$ by the scanning potential from − 0.2–0.6 V with scan rates from a to m as 20, 40, 60, 80, 100, 200, 300, 400, 500, 600, 700, 800 and 900 mV s^{-1}, respectively (Inset: linear relationship of E_{pa} (the black line) and E_{pc} (the red line) versus lg υ). (For interpretation of the references to color in this figure legend, the reader is referred to the web version of this article.)

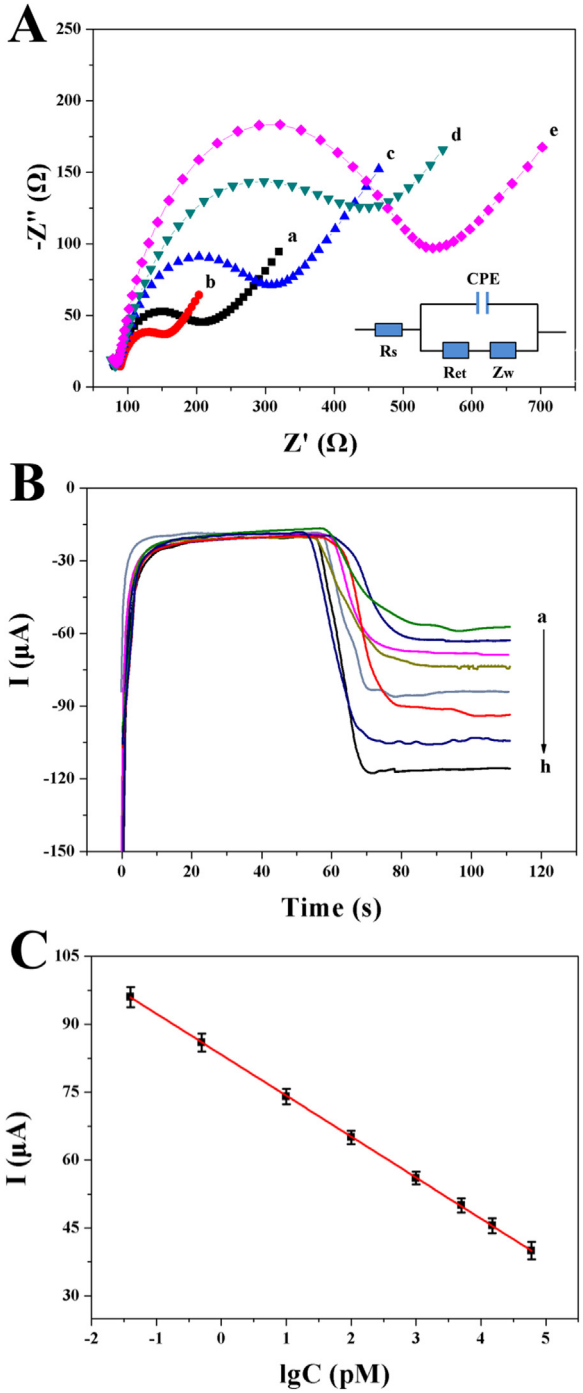

Fig. 4. (A) Nyquist plots of the A.C. impedance method: GCE (a), TiO_2-NGO/Au@Pd HSs/GCE (b), anti-HE4/TiO_2-NGO/Au@Pd HSs/GCE (c), BSA/anti-HE4/TiO_2-NGO/Au@Pd HSs/GCE (d), HE4 Ag/BSA/anti-HE4/TiO_2-NGO/Au@Pd HSs/GCE (e), represented as Randles equivalent circuit for A.C. impedance (inset); (B) Amperometric responses of the immunosensor for the detection of different concentrations of HE4 Ag: 60 nM (a), 5 nM (b), 1 nM (c), 100 pM (d), 10 pM (e), 5 pM (f), 60 fM (g), 40 fM (h); (C) Calibration curve of the immunosensor for the detection of different concentrations of HE4 Ag. Error bar = RSD (n = 5).

the bioactive substances.

3.4. Analytical performance of immunosensor

To obtain the best analytical performance for HE4 Ag, various experiment conditions were optimized including the pH of PBS,

concentration of TiO_2-NGO/Au@Pd HSs and the incubation time between antigen and antibody, and the optimum value is 7.4, 2.5 mg mL^{-1} and 40 min respectively (Fig. S5). The detail information was provided in SM. Under optimum conditions, we detected a series concentration of HE4 Ag by i-t measurement using TiO_2-NGO/Au@Pd HSs hetero-nanostructures as the signal amplification platform. With the increase of the HE4 Ag concentrations, the current signal responses of the immunosensor declined, implying that antigen hindered electron transport (Fig. 4B). The linear regression equations between the current response and the logarithm of the HE4 Ag concentration in the range from 40 fM to 60 nM was $I = -9.06\ lgC + 83.29$, with a correlation coefficient of 0.9999. The limit of detection (LOD) of HE4 Ag was 13.33 fM (S/N = 3).

In comparison to the results of other reported immunosensors for detecting HE4 Ag (Table S3), the designed immunosensor exhibited an improved LOD (13.33 fM) and comparable linear range (40 fM–60 nM). The reasons why the prepared immunosensor provides a lower detection limit are as follows. Firstly, the TiO_2-NGO/Au@Pd HSs hetero-nanostructures have good biocompatibility to ensure the activity of biological proteins and can immobilize antibodies effectively. Secondly, the multiple signal amplification platforms can provide wider detection range. Finally, the TiO_2-NGO/Au@Pd HSs hetero-nanostructures have good electron transfer properties which can improve the sensitivity of the immunosensor.

3.5. Evaluation of the repeatability, specificity and stability, of the immunosensor

The reproducibility and stability of the immunosensor are the key factors in the application of the immunosensor. A series of working electrodes were constructed and divided into three groups (five electrodes each group) to detect 1 nM,10 pM and 40 fM of HE4 Ag, respectively (Fig. 5A). The relative standard deviation (RSD) values were 2.1%, 1.9% and 2.3%, which indicated a good reproducibility for the HE4 Ag immunosensor.

The specificity of target analysis plays a vital role in analyzing biological samples. Interfering substances including carcinoembryonic antigen (CEA), immunoglobulin G (IgG), BSA and carbohydrate antigen 125 (CA 125) were added into 1 nM of HE4 Ag solutions. The current change was less than 5.0% of that without interference (Fig. 5B), indicating the acceptable specificity.

For evaluation of the stability, the prepared immunosensor was stored in 4 °C with the current response being tested per week. The signal value retained 90.2% of its original value after a storage period of four weeks (Fig. 5C). This result indicated that the stability of the proposed immunosensor was acceptable. Also, Fig. S6 further illustrated the stability of the immunosensor was satiable.

3.6. Real sample analysis

To test the potential of the prepared immunosensor for practical analysis, the recoveries of different concentrations of HE4 Ag in human serum samples were conducted by standard addition recovery method (Bo and Kowalski, 1979). As is listed in Table 1, the recovery and RSD value were obtained between 99.8% and 100.16% and 0.3–1.59% respectively, which indicated that the immunosensor supplies a feasible approach for clinical research.

To validate the prepared immunosensor, the electrochemiluminescence immunoassay (ECLIA) was compared, as is shown in Table S4. The relative error between the two methods is in the range from 1.81% to 2.36%. This result indicates that the proposed immunosensor is promising for clinical application.

4. Conclusions

In this study, an ultrasensitive label-free electrochemical immunosensor was designed successfully and realized the quantitative determination of HE4 Ag. The novel multi-amplification signal strategy of TiO_2-NGO/Au@Pd HSs hetero-nanostructures with the good conductivity, large surface area and excellent electrocatalytic activity not only acts as the support for the immunologic material but also a transducer to enhance the sensitivity of the immunosensor. Overall, the prepared label-free electrochemical immunosensor possesses good reproducibility, specificity and acceptable stability. This proposed strategy might have a promising application for other biomolecules in clinical diagnosis.

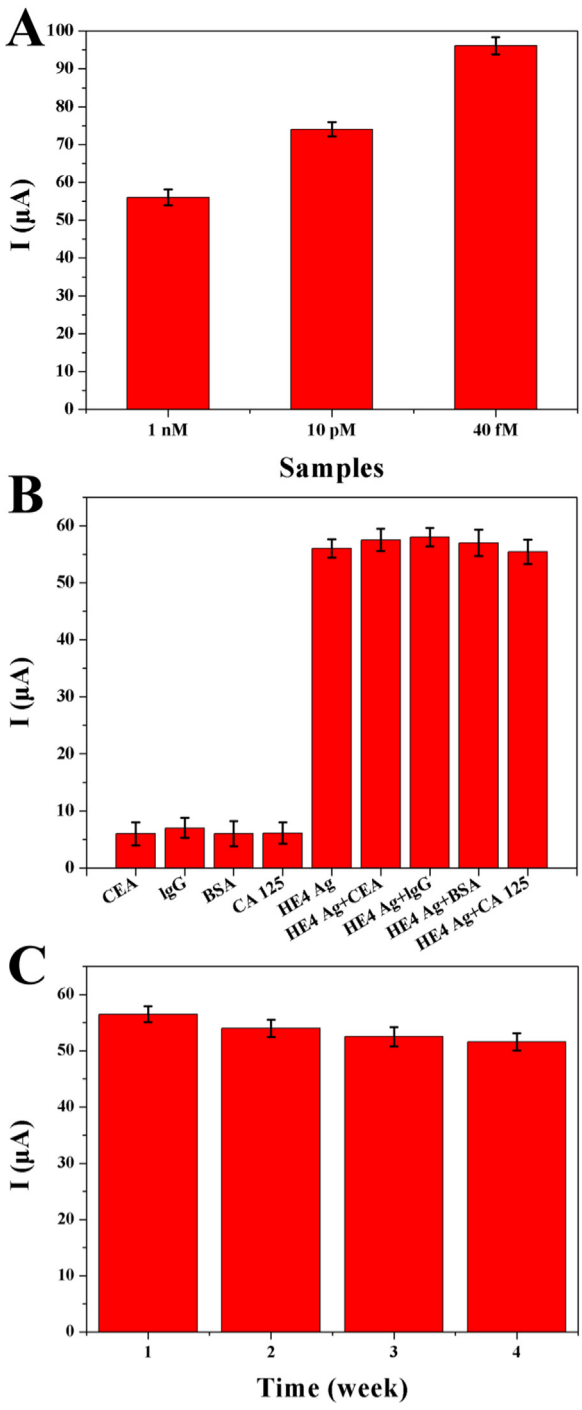

Fig. 5. (A) Amperometric response of the immunosensor to detect 1 nM, 10 pM and 40 fM of HE4 Ag; (B) The current of interfering substances (50 nM) alone and compound of interfering substances and HE4 Ag (1 nM); (C) Stability study of the immunosensor in 4 weeks. Error bar = RSD (n = 5).

Table 1
Detection of the HE4 Ag in human serum samples with the proposed immunosensor.

Content of HE4 Ag in the serum (nM)	The addition content (nM)	The detection content (nM)	RSD (%, n = 5)	Recovery (%)
0.50	1.00	1.48, 1.51, 1.50, 1.47, 1.53	1.59	99.8
0.50	5.00	5.52, 5.54, 5.47, 5.48, 5.53	0.57	100.16
0.50	10.00	10.44, 10.5, 10.51, 10.48, 10.52	0.30	99.90

CRediT authorship contribution statement

Qin Yan: Conceptualization, Data curation, Investigation, Methodology, Software, Writing - original draft, Writing - review & editing. **Linlin Cao:** Data curation, Resources, Writing - original draft. **Hui Dong:** Data curation, Investigation, Visualization. **Zhaoling Tan:** Investigation, Writing - review & editing. **Yitian Hu:** Formal analysis, Investigation, Validation. **Qing Liu:** Conceptualization, Data curation, Funding acquisition, Project administration, Resources, Supervision, Visualization. **Hui Liu:** Project administration, Resources, Supervision, Validation. **Pingping Zhao:** Resources, Validation, Writing - review & editing. **Lei Chen:** Validation, Writing - review & editing. **Yuying Liu:** Data curation, Resources, Software, Validation. **Yueyun Li:** Resources, Supervision, Validation. **Yunhui Dong:** Resources, Supervision, Validation.

Acknowledgment

We greatly appreciate the support of the National Natural Science Foundation of China (21405095; 21575079), CPSF (2016M590736) and Special Funding for Postdoctoral Innovation Project of Shandong Province (201501002), the Young Talents Joint Fund of Shandong Province (ZR2015JL005), CPSF (2016M590736), the Key Research and Development Program of Shandong Province (2018GSF120001).

Declaration of interest statement

None.

Appendix A. Supplementary material

Supplementary data associated with this article can be found in the online version at doi:10.1016/j.bios.2018.12.038.

References

Akhtar, N., El-Safty, S.A., Abdelsalam, M.E., Kawarada, H., 2015. Adv. Healthc. Mater. 4, 2110–2119.
Akhtar, N., El-Safty, S.A., Abdelsalam, M.E., Shenashen, M.A., Kawarada, H., 2016. Biosens. Bioelectron. 77, 656–665.
Akhtar N, E.M.Y., Shenashen, M.A., et al., 2017. J. Mater. Chem. B 5, 7985–7996.
Alarfaj, N.A., Eltohamy, M.F., Oraby, H., 2018. New J. Chem.
Anastasi, E., Marchei, G.G., Viggiani, V., Gennarini, G., Frati, L., Reale, M.G., 2010. Tumor Biol. 31, 113–119.
Balachandran, U., Eror, N.G., 1982. J. Solid State Chem. 42, 276–282.
Berggren, C., Johansson, G., 1997. Anal. Chem. 69, 3651–3657.
Bo, E.H.S., Kowalski, B.R., 1979. Anal. Chem. 51, 1031–1038.
Capriglione, S., Plotti, F., Miranda, A., Lopez, S., Scaletta, G., Moncelli, M., Luvero, D., Nardone, C.D.C., Terranova, C., Montera, R., 2017. Expert Rev. Anticancer Ther. 17, 9–18.
Chen, Shihong, Yuan, Chai, Yaqin, Hu, Fangxin, 2013. Microchim. Acta 180, 15–32.
Chen, X., Mao, S.S., 2007. Chem. Rev. 107, 2891–2959.
Daniel, M.C., Astruc, D., 2004. Chem. Rev. 35, 293–346.
Emran, M.Y., Khalifa, H., Gomaa, H., Shenashen, M.A., Akhtar, N., Mekawy, M., Faheem, A., El-Safty, S.A., 2017a. Microchim. Acta 184, 4553–4562.
Emran, M.Y., Mekawy, M., Akhtar, N., Shenashen, M.A., El-Sewify, I.M., Faheem, A., El-Safty, S.A., 2017b. Biosens. Bioelectron. 100, 122–131.
Emran, M.Y., Shenashen, M., Abdelwahab, A.A., Abdelmottaleb, M., El-Safty, S., 2018a. New J. Chem.
Emran, M.Y., Shenashen, M.A., Morita, H., El-Safty, S.A., 2018b. Biosens. Bioelectron. 109, 237.
Felix, F.S., Angnes, L., 2017. Biosens. Bioelectron. 98, 470–478.
Ghasemi, S., Esfandiar, A., Setayesh, S.R., Habibi-Yangjeh, A., Zad, A.I., Gholami, M.R., 2013. Appl. Catal. A General. 462–463, 82–90.
Kaur, M., Kaur, M., Sharma, V.K., 2018. Adv. Colloid Interface Sci. 259, 44–64.
Kim, J., Song, X., Fei, J., Luo, B., Ice, N.F., Liu, Q., Qiao, Z., Qian, C., 2017. Nano Lett. 17.
Kim, J.H., Jeong, H.M., Chan, W.N., Yoon, J.W., Abdel-Hady, F., Wazzan, A.A., Lee, J.H., 2016. Sens. Actuators B Chem. 235, 498–506.
Laviron, E., 1979. J. Electroanal. Chem. Interfacial Electrochem. 100, 263–270.
Laviron, E., Roullier, L., 1980. J. Electroanal. Chem. 115, 65–74.
Li, F., Li, Y., Feng, J., Gao, Z., Lv, H., Ren, X., Wei, Q., 2018a. Biosens. Bioelectron. 100, 512–518.
Li, L., Dechesne, A., He, Z., Madsen, J.S., Nesme, J., Sørensen, S.J., Smets, B.F., 2018b. Environ. Sci. Technol. Lett. 5, 260–265.
Li, Q., Luo, G., Feng, J., 2015. Electroanalysis 13, 359–363.
Li, Y., Zhang, Y., Li, F., Feng, J., Li, M., Lei, C., Dong, Y., 2017. Biosens. Bioelectron. 92, 33.
Liu, H., Chen, Z., Zhang, L., Zhu, D., Zhang, Q., Luo, Y., Shao, X., 2018. J. Phys. Chem. C.
Lu, K.H., 2018. JAMA 319, 557.
Dal Magro, P., S, C.F., Gnanamani, A., 2018. RSC Adv. 8, 38416–38424.
Mathieu, K.B., Bedi, D.G., Thrower, S.L., Qayyum, A., Bast, R.C., 2017. Ultrasound Obstet. Gynecol. 51, 293–303.
Nosrati, R., Olad, A., Shakoori, S., 2017. Mater. Sci. Eng. C. 80, 642–651.
Okuno, J., Maehashi, K., Kerman, K., Takamura, Y., Matsumoto, K., Tamiya, E., 2007. Biosens. Bioelectron. 22, 2377–2381.
Qamar, M., Merzougui, B., Ahmed, M.I., Yamani, Z.H., 2017. Acs Sustain. Chem. Eng. 6, 2112–2121.
Rauf, S., Mishra, G.K., Azhar, J., Mishra, R.K., Goud, K.Y., Nawaz, M., Marty, J.L., Hayat, A., 2018a. Anal. Biochem. 545, 13–19.
Rauf, S., Mishra, G.K., Azhar, J., Mishra, R.K., Goud, K.Y., Nawaz, M., Marty, J.L., Hayat, A., 2018b. Anal. Biochem. 545.
Samanman, S., Numnuam, A., Limbut, W., Kanatharana, P., Thavarungkul, P., 2015. Anal. Chim. Acta 853, 521–532.
Sengottaiyan, C., Jayavel, R., Bairi, P., Shrestha, R.G., Ariga, K., Shrestha, L.K., 2017. Bull. Chem. Soc. Jpn. 90, 955–962.
Swamy, V., Kuznetsov, A., Dubrovinsky, L.S., Caruso, R.A., Shchukin, D.G., Muddle, B.C., 2005. Phys. Rev. B 71 (184302), 184301–184311.
Tran, T.T., Lu, X., 2011. J. Phys. Chem. C. 115, 3638–3645.
Wang, F., Li, C., Sun, L.D., Wu, H., Ming, T., Wang, J., Yu, J.C., Yan, C.H., 2011. J. Am. Chem. Soc. 133, 1106–1111.
Wang, H., Chai, Y., Li, H., Yuan, R., 2017a. Biosens. Bioelectron. 100, 35–40.
Wang, R., Wang, A.J., Liu, W.D., Yuan, P.X., Xue, Y., Luo, X., Feng, J.J., 2017b. Biosens. Bioelectron. 102, 276–281.
Wei, Q., Zhao, Y., Du, B., Wu, D., Li, H., Yang, M., 2012. Food Chem. 134, 1601–1606.
Wei, Y., Li, Y., Li, N., Zhang, Y., Yan, T., Ma, H., Wei, Q., 2016a. Biosens. Bioelectron. 79, 482–487.
Wei, Y., Yan, L., Na, L., Yong, Z., Tao, Y., Ma, H., Qin, W., 2016b. Biosens. Bioelectron. 79, 482–487.
Yan, Q., Yang, Y., Tan, Z., Liu, Q., Liu, H., Wang, P., Chen, L., Zhang, D., Li, Y., Dong, Y., 2018. Biosens. Bioelectron. 103, 151–157.
Yang, M., Cheng, K., Qi, S., Liu, H., Jiang, Y., Jiang, H., Li, J., Chen, K., Zhang, H., Cheng, Z., 2013. Biomaterials 34, 2796–2806.
Yang, Y., Liu, Q., Liu, Y., Cui, J., Liu, H., Wang, P., Li, Y., Chen, L., Zhao, Z., Dong, Y., 2016. Biosens. Bioelectron. 90, 31–38.
Yang, Y., Qin, Y., Liu, Q., Li, Y., Hui, L., Ping, W., Lei, C., Zhang, D., Li, Y., Dong, Y., 2017a. Biosens. Bioelectron. 99, 450–457.
Yang, Z., Lan, Q., Li, J., Wu, J., Tang, Y., Hu, X., 2017b. Biosens. Bioelectron. 89, 312–318.
Yao, L., Liu, J., Duan, B., Hou, M., Tamirat, A.G., Wang, Y., Xia, Y., 2018. Acs Appl. Mater. Interfaces 10, 14818–14826.
Yu, J., Liu, Z., Zhai, L., Huang, T., Han, J., 2016. Int. J. Hydrog. Energy 41, 3436–3445.
Zhang, L., Conejogarcia, J.R., Katsaros, D., Gimotty, P.A., Massobrio, M., Regnani, G., Makrigiannakis, A., Gray, H., Schlienger, K., Liebman, M.N., 2003. N. Engl. J. Med. 348, 203–213.
Zhang, L., Jiang, X., Wang, E., Dong, S., 2006. Biosens. Bioelectron. 21, 337–345.
Zhang, X., Sun, Z., Wang, B., Tang, Y., Luan, N., Li, Y., Tao, F.F., 2018. J. Am. Chem. Soc. 140, 954.
Zhao, Y.D., Bi, Y.H., Zhang, W.D., Luo, Q.M., 2005. Talanta 65, 489–494.
Zhou, Y., Zhuo, Y., Liao, N., Chai, Y., Yuan, R., 2014. Chem. Commun. 50, 14627–14630.